Spin dynamics of the anisotropic spin-1 antiferromagnetic chain at finite magnetic fields

Yousef Rahnavard and Wolfram Brenig
Institut für Theoretische Physik, Technische Universität Braunschweig, 38106 Braunschweig, Germany
(Received 29 November 2014; revised manuscript received 25 January 2015; published 12 February 2015)

We present results of a study of the antiferromagnetic spin-1 chain, subject to the simultaneous presence of single-ion anisotropy and external magnetic fields. Using a quantum Monte Carlo calculation based on the stochastic series expansion method, we first uncover a rich quantum phase diagram comprising Néel, Haldane, Luttinger-liquid, and large-anisotropy phases. Second, we scan across this phase diagram over a wide range of parameters, evaluating the transverse dynamic structure factor, which we show to exhibit sharp massive modes as well as multiparticle continua. For vanishing anisotropy and fields, comparison with existing results from other analytic and numerical approaches shows convincing consistency.

DOI: 10.1103/PhysRevB.91.054405 PACS number(s): 75.10.Jm, 75.40.Gb, 75.50.Ee, 75.40.Mg

I. INTRODUCTION

Ever since Haldane's conjecture [1] on the difference between even and odd half-integer Heisenberg antiferromagnetic spin chains (HAFCs), the spin-1 HAFC (S1-HAFC)

$$H = J\sum_{l=1}^{L}\vec{S}_l\cdot\vec{S}_{l+1} - h\sum_{l=1}^{L}S_l^z + D\sum_{l=1}^{L}\left(S_l^z\right)^2, \qquad (1)$$

has been considered to be one of the fundamental models of low-dimensional quantum magnetism. The first term on the right-hand side of (1) refers to the *bare* chain, with antiferromagnetic exchange interaction J and spin-1 operators $\vec{S}_l$ at sites l, and the remaining terms capture common perturbations by single-ion anisotropy D and external longitudinal magnetic fields h.

For the isotropic case at zero magnetic field, i.e., $D = 0$ and $h = 0$, both static and dynamic properties of the S1-HAFC have been investigated extensively using various theoretical and numerical methods [2]. On the zone boundary at $q = \pi$, its lowest-lying excitation is a massive "single-magnon" mode which displays the famous Haldane gap of $\Delta \simeq 0.41J$ [3,4]. Near $q = 0$ the spectrum comprises primarily a two-particle continuum of small spectral weight [4–7]. This continuum is separated from the ground state by 2Δ. Finally, the next-to-dominant excitations near $q = \pi$ are contained in a three-particle continuum starting at 3Δ. Theoretically, these excitations have been obtained from several analytic approaches, e.g., mean-field theory [6], the nonlinear σ model (NLσM) [8], as well as numerical methods, e.g., quantum Monte-Carlo (QMC) simulation [9–12] and the density matrix renormalization group (DMRG) [4,13].

Experimentally, the massive magnon at $q = \pi$ has been confirmed irrevocably; however, the two- and in particular the three-particle continua remain a matter of active research [14–16].

Most spin-1 chain compounds, such as $Ni(C_2H_8N_2)_2NO_2(ClO_4)$ (NENP) [17,18], $NiCl_2.4SC(NH_2)_2$ (DTN) [19,20], $Ni(C_2H_8N_2)_2Ni(CN)_4$ (NENC) [21], $Ni(C_5H_{14}N_2)_2N_3(PF_6)$ (NDMAP) [22,23], and $Ni(C_5H_{14}N_2)_2N_3(ClO_4)$ (NDMAZ) [24,25] display sizable anisotropy D and even the well-studied prototype material $CsNiCl_3$ [26,27] has $D \neq 0$. Therefore, it is of great interest to analyze the ground-state properties and the evolution of the excitation spectrum as a function of anisotropy. In addition, many experimental studies, including neutron scattering [18,28], electron-spin resonance [29,30], nuclear magnetic resonance [31–33], and thermal transport [34] are performed at finite magnetic fields.

For vanishing magnetic field several studies have already been performed regarding the quantum phases as a function of the anisotropy [35–43]. Similarly the magnetic-field-driven transition into a Luttinger-liquid (LLQ) phase [44–46] at $D = 0$ is well investigated. At finite D *and* h, there are some studies with planar or a combination of planar and axial magnetic fields and additional other components of anisotropies [47–49], still too little is known about the region of finite D and h for the Hamiltonian (1). Therefore, the central goal of this paper is to shed more light onto the combined impact and interplay between finite anisotropy and magnetic fields in S1-HAFCs, regarding both static and dynamic properties.

The paper is organized as follows. In Sec. II we uncover and discuss the quantum phase diagram of (1) over a substantial range of D and h. In Sec. III we detail our results for the transverse dynamic structure factor (TDSF) and analyze its evolution in terms of anisotropy and magnetic fields. Where available comparison to other methods, in particular NLσM model calculations [6,8] and TDMRG [13] will be provided. We conclude and summarize our findings in Sec. IV. The Appendix contains a short summary of the quantum Monte Carlo method we use.

II. QUANTUM PHASE DIAGRAM

In this section, and before analyzing its dynamical properties, we will evaluate the ground-state phase diagram of the chain versus single-ion anisotropy and magnetic field. At zero magnetic field, the phase diagram in terms of anisotropy has already been investigated [35–38]. It consists of a Néel, a Haldane, and a large-D phase. The transition from the Néel to the Haldane phase is of Ising type, while that from the Haldane to the large-D phase is of Gaussian type. The critical values D_c for the transition between these phases have been determined using various numerical methods, including exact diagonalization [38], DMRG [39–41], series expansions, and QMC simulation [43]. Although there are slight quantitative differences between the results from different methods for D_c, it is generally believed that the transition between the

Néel and Haldane phases occurs around $D_{NH} \simeq -0.31J$ and that between the Haldane and large-D phases around $D_{HL} \simeq 1.0J$ [39–41,43].

All three phases, namely, Néel, Haldane, and large D, are gapful. It is known that the spin gap of the Haldane phase decreases upon increasing the easy-plane anisotropy up to the critical point D_c and increases again afterwards; however, one remains in a gapful state [41]. Application of an external magnetic field can also suppress the spin gap of the chain [44–46], resulting in a gap closure and a transition into a LLQ at a critical field h_c which depends on D. Both field-driven transitions, i.e., from the Haldane [44,50] and from the large-D [51] phase into the LLQ can be viewed as one-dimensional (1D) analogs of 3D Bose-Einstein condensation or the 2D Berezinsky-Kosterlitz-Thouless transition), with no true condensate but algebraic correlation functions transverse to the field [44]. The transition line $h_c(D)$ is not known, apart from low-order series expansions, valid for $D/J \gg 1$ for the large-D to LLQ case [51].

Our aim will be to extract the LLQ boundaries at intermediate h/J and D/J, thereby establishing how the quantum phases evolve within the D-h plane. There are several ways to determine the extent of the Haldane phase. One is to evaluate the string order parameter [35,37], which is a nonlocal probe of the topological order. This order parameter is fragile with respect to perturbations which break rotation symmetry, while keeping other symmetries such as time-reversal, parity, and translation symmetries intact [47,48,52]. Since both the Haldane and large-D phases are gapped while the LLQ formed between them is gapless, another and rather direct way to determine the boundary between these phases is to scan the energy gap versus D, fixing, e.g., h. To obtain the gap, we first evaluate the uniform spin susceptibility in terms of temperature, $\chi(T)$. We then extract the gap by fitting the low-temperature values of $\chi(T)$ to $\chi(T) \approx e^{-\Delta/T} P_k^l(T)/T$, where $P_k^l(T)$ is a Padé approximant of order $[k,l]$. In principle, finite-size scaling of the gap determined in this way should be performed, in particular because of critical behavior near the transition points [53]. In practice however and because of the additional approximation introduced by the Padé fitting, we simply use a sufficiently large system of 512 sites with periodic boundary conditions (PBCs) imposed throughout this work. The lowest temperature we have considered is $T = 0.0078J$.

Figure 1 summarizes all gaps $\Delta(D,h)$ extracted from the preceding procedure, both versus D and for several magnetic fields. For each gap, the Padé fitting errors are found to be within the QMC calculation's error bars which are of the order of 10^{-4}. Above the critical field $h_c(D)$, there are two points of gap closure and reopening, which we identify with the transition from the Haldane into the LLQ, and from the LLQ into the large-D phase. At $D = D_{HL}$ the latter two points have to merge at $h = 0$ where the direct transition from the Haldane to large-D phase occurs without accessing a LLQ phase. The gaps in Fig. 1 display some clearly visible, albeit small noise. This is not related to QMC or Padé approximant errors. Rather, the noise is a consequence of the arbitrariness in choosing the upper cutoff for the temperature range, used in Padé fitting $\chi(T)$. This noise translates into an error for the phase boundaries, which we find to dominate any corrections from finite scaling. This justifies our neglect of the latter *a posteriori*.

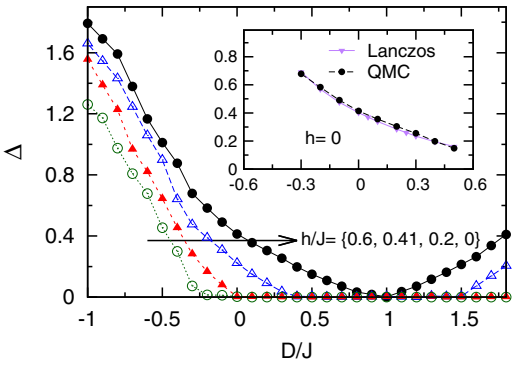

FIG. 1. (Color online) Spin gap of the spin-1 chain in terms of single-ion anisotropy for different external magnetic fields. Inset: For zero magnetic field, the spin gap in terms of single-ion anisotropy obtained from the QMC and Lanczos methods is shown. Lanczos data are extracted from Ref. [42]. The system size and the lowest temperature considered for QMC data are $L = 512$ and $T = 0.0078$.

Previous studies [42] have analyzed the spin gap for $h = 0$ using Lanczos spectra of small systems $L \leqslant 20$, over a restricted range of $D_{NH} < D < D_{HL}$. As compared to QMC calculations, finite-size effects are a relevant issue for this approach, and careful scaling analysis is necessary, in particular for D in the vicinity of D_{HL}, where gap closure occurs. The inset of Fig. 1 compares our thermodynamic QMC gap with that obtained from extrapolating to $L \to \infty$ in Ref. [42]. The agreement is satisfying.

In Fig. 2, we collect the gap closure points obtained from Fig. 1 as part of a quantum phase diagram versus D and h. The transition points are regarded as the midpoints of the two sequential D values for one of which Δ is finite (gapped phase) while for the other one $\Delta \approx 0$ (gapless phase). Since the distance between two sequential D/J values is 0.1, the uncertainty for the transition points is ± 0.05. The lines connecting the points are low-order polynomials fitted to the points. This figure also shows a transition from the Néel to the Haldane phase, to which we turn now. Since both of the latter phases are gapful, the transition line cannot be obtained

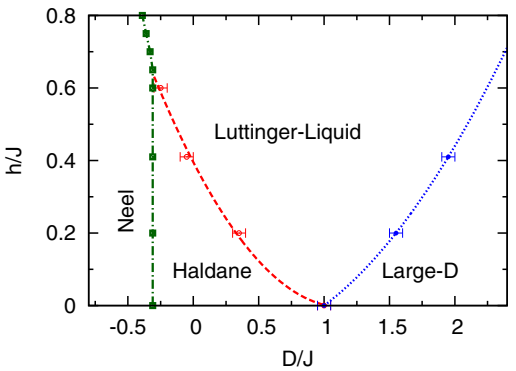

FIG. 2. (Color online) Quantum phase diagram of the spin-1 Heisenberg chain versus single-ion anisotropy and magnetic field. The error bars of the transition points are equal to the distance between two sequential values of D/J in each of the two procedures, gap or Néel order study. In the Haldane-Néel case, these error bars are smaller than the symbols.

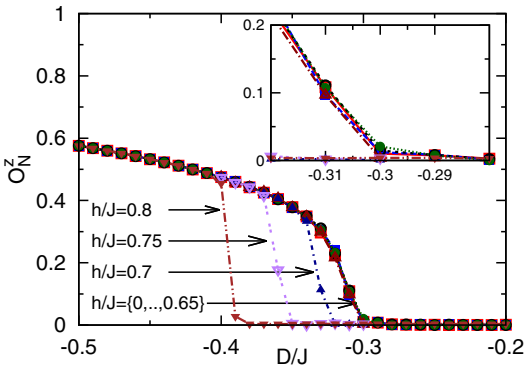

FIG. 3. (Color online) Néel order parameter is shown as a function of anisotropy for different magnetic fields. The inset shows the transition point between Haldane and Néel phases for $h/J = 0, \ldots, 0.65$. The system size and the temperature considered here are $L = 512$ and $T = 0.01J$.

from a study of gap closures. Instead, we use the fact that the long-range staggered spin correlation is an order parameter of the Néel phase, and remains finite therein, while it decays in the Haldane phase [54]. This has been applied previously to characterize the Haldane phase as a function of exchange anisotropy in the XXZ spin-1 chain [55]. The staggered spin correlation reads

$$\mathcal{O}_{\mathrm{N}}^{z}(i,j) = (-1)^{i-j}\langle S_i^z S_j^z\rangle, \tag{2}$$

and Néel ordering implies $O_{\mathrm{N}}^{z} = \lim_{|i-j|\to\infty} \mathcal{O}_{\mathrm{N}}^{z}(i,j) \neq 0$.

Due to the PBCs the largest proper distance on the chain is $L/2$. Figure 3 displays our results for $\mathcal{O}_{\mathrm{N}}^{z}(0,L/2)$ with $L = 512$. In view of the rather large system, we refrain from finite-size scaling analysis and approximate $O_{\mathrm{N}}^{z} \simeq \mathcal{O}_{\mathrm{N}}^{z}(0,L/2)$. We identify the phase transition point with the average value between the smallest D at which $O_{\mathrm{N}}^{z} \approx 0$, where we are in the Haldane phase, and the largest D point at which O_{N}^{z} is finite, where we are in the Néel phase. The error in this case is ± 0.005. From this and for $h = 0$, we obtain a transition point at $D_{NH} \approx -0.305J$, which is satisfyingly close to the values obtained by DMRG in Refs. [40,41].

The main message of Fig. 3 is contained in the remarkable evolution of O_{N}^{z} and the quantum critical point with magnetic field. As the figure shows, the critical value of $D_{NH}(h)$ is independent of the field up to a critical value $\tilde{h}/J \approx 0.65$, below which all curves for O_{N}^{z} collapse onto a single one. Adding $D_{NH}(h)$ into Fig. 2 shows that the point $(D_{NH},\tilde{h})$ lies on the extrapolated line, approximating the boundary of the LLQ phase. From the slope of this phase boundary, and since O_{N}^{z} has to be zero in the LLQ phase, further increasing the field, the value of $D_{NH}(h)$ must decrease for $h > \tilde{h}$. This is consistent with O_{N}^{z} in Fig. 3. In fact, as is obvious from the green squares in Fig. 2, to within the uncertainty of the LLQ phase boundary, the Néel-Haldane transition is replaced by a direct transition from the Néel to the Luttinger-liquid phase for $h > \tilde{h}$. This corresponds to a direct transition from a state with broken Z_2 symmetry to one with algebraically decaying fluctuations transverse to the field. From Fig. 3 it seems that the Néel order parameter decreased continuously for $h < \tilde{h}$, while for the direct Néel to LLQ transition our data could also be consistent with a (weakly) first-order jump of O_{N}^{z}, in particular for larger fields. Clearly this transition requires more studies.

III. DYNAMIC STRUCTURE FACTOR

In this section we discuss the following transverse dynamic structure factor:

$$S^{xx}(q,\omega) = \int_{-\infty}^{\infty} dt\, e^{i\omega t} S^{xx}(q,t), \tag{3}$$

where q refers to momentum, ω to frequency, t to real time, and $S^{xx}(q,t) = \langle S_q^x(t) S_{-q}^x\rangle$, with $S_q^x = \sum_l e^{-iql} S_l^x$. Details of how to obtained this quantity from QMC data are contained in the Appendix. For brevity we will denote $S(q,\omega) \equiv S^{xx}(q,\omega)$. We will be interested in the Néel, Haldane, and Luttinger-liquid phases. For this we analyze several values of magnetic field and anisotropy, as shown in Fig. 2.

First, we focus on the field dependence of $S(q,\omega)$ at the isotropic point. Results for this are shown in the contour plots of Fig. 4. At zero magnetic field most of the spectral weight is contained in a single, well-defined excitation, which is clearly visible in Fig. 4(a). Most of the spectral weight of this so-called one-magnon mode resides at large momenta near $q = \pi$ and decreases rapidly towards lower momenta, where we find that the integrated weight is proportional to q^2 as $q \to 0$. At finite magnetic field, the two triplet branches which can be reached by $\Delta S = +1$ transitions split according to their Zeeman energy. For small fields, this splitting is

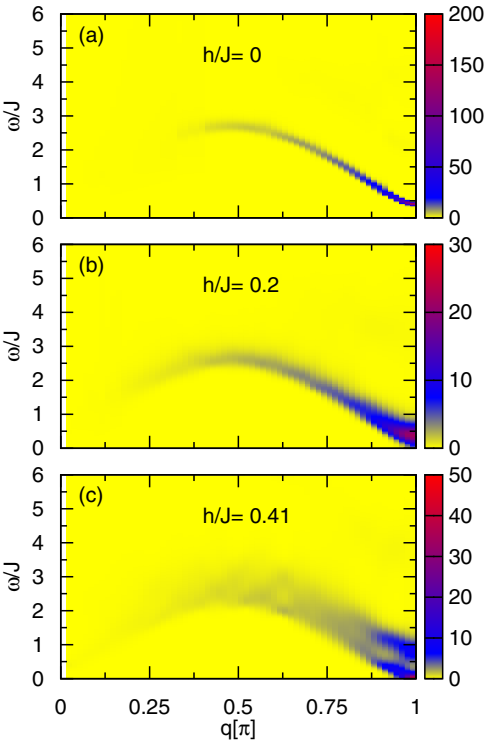

FIG. 4. (Color online) Contour plot of the transverse dynamic structure factor of the isotropic spin-1 chain as a function of frequency ω and wave vector q for three different magnetic fields $h = 0$, $0.2J$, and $0.41J$. The system size of the chain for all cases is $L = 128$ and the temperature is set to $T = 0.1J$.

manifest through a broadening of the one-magnon line, while the intensity decreases, as can been seen from Fig. 4(b) and by comparing their intensity scales. If the Zeeman splitting is larger than the broadening of the one-magnon excitations due to thermal, interaction, and maximum entropy (MaxEnt) effects, then the splitting is directly visible, as in Fig. 4(c). In that panel, the Zeeman energy has been chosen identical to the Haldane gap. As can be seen, at this point the maximum intensity of the lower branch extrapolates to zero energy at $q = \pi$, i.e., the gap closes, consistent with entering the LLQ phase.

Next we focus on a more detailed discussion of 2D cuts of the spectra versus D and h at small and large momenta. The main motivation for this is that apart from the one-magnon excitation, there are also multiparticle continua present in the spectrum. While the former are most dominant at large momenta, the latter exhibit very small spectral weight, which remains invisible in contour plots of the full Brillouin zone (BZ), and can be observed best at small momenta. Therefore we have plotted cuts through the TDSFs at various anisotropies and magnetic fields in Fig. 5, which allows the shape and weight of the spectra to be clearly seen, despite very large differences in their absolute scales in different frequency and momentum regions. We have chosen three magnetic fields $h/J = \{0,0.2,0.41\}$ and five different anisotropies $D/J = \{-0.5,-0.2,0,0.2,0.5\}$, ranging from easy-axis to easy-plane

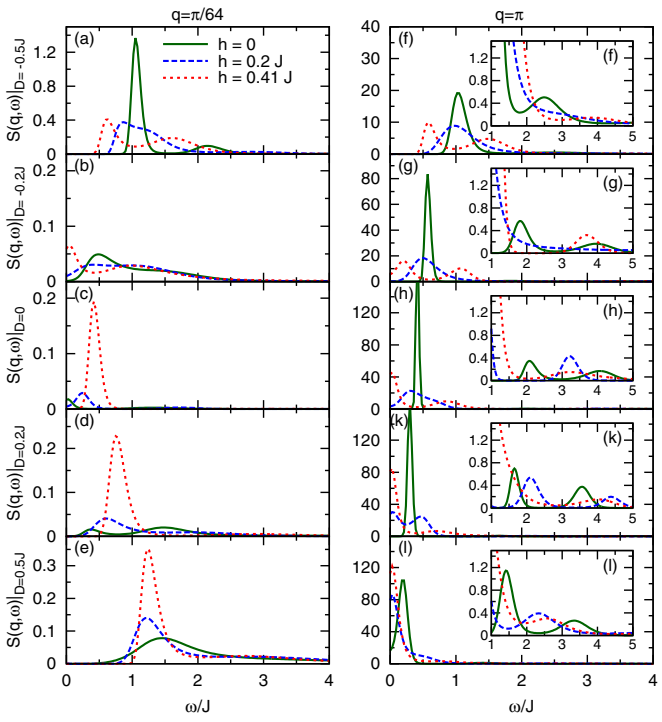

FIG. 5. (Color online) Transverse dynamic structure factor of the spin-1 chain, $S(q,\omega)$, as a function of frequency at two momenta, $q = \pi/64$ (left panels) and $q = \pi$ (right panels), for three magnetic fields $h/J = \{0,0.2,0.41\}$ and five different anisotropies $D/J = \{-0.5,-0.2,0,0.2,0.5\}$ corresponding to panels (a)–(e) and (f)–(l), respectively. The insets in (f)–(l) show the large-frequency spectra at $q = \pi$. The system size of the chain for all cases is $L = 128$ and the temperature is set to $T = 0.1J$.

anisotropies. For each of these cases two wave vectors have been considered, i.e., $q = \pi$ (right panel), and $q = \pi/64$ (left panel), which is the smallest on the system for which we have evaluated the TDSF, i.e., $L = 128$.

We start with the isotropic case at small momenta, Fig. 5(c). At zero magnetic field it is dominated by a peak at zero frequency. This *central peak* intensity stems from $\Delta S = +1$ transitions within thermally excited states and decreases as the temperature is lowered. In addition, there exists a continuum of very small weight at higher frequencies, which, however, is not observable on the scale of this plot. We emphasize that this observation is rather distinct from expectations [13] at *zero* temperature, where the latter multimagnon spectrum should dominate the spectrum at low momentum, displaying a gap of twice the Haldane gap. On increasing the wave vector, the weight of the continuum gets larger, as we will discuss later. On increasing the magnetic field, the central peak and the continuum shift to larger frequencies, with an energy scale set by the Zeeman energy.

Turning to finite anisotropy either of easy-axis type in Figs. 5(a) and 5(b) or of easy-plane type in Figs. 5(d) and 5(e), a shifting of the dominant weight of the spectrum to larger frequencies is clearly visible. In addition to that, an interesting interplay between the effects of anisotropy and magnetic field on the spectrum can be observed, which differs between the two kinds of anisotropies. While in the case of easy-plane anisotropy, the magnetic field only slightly shifts the weight of the spectrum, in the case of easy-axis anisotropy, a splitting of the dominant peak results which increases with increasing field.

Another interesting feature is the evolution of the spectrum versus anisotropy upon switching from the Haldane into the Néel phase. In the former we expect a rather broad continuum from multiparticle excitations at small momentum, while in the latter a single dominant excitation should occur, representing one-magnon excitations, which may however still exhibit some broadening due to finite-temperature and interaction effects. Exactly this can be seen in going from Figs. 5(b) to 5(a), where also the overall amplitude scale increases by one order of magnitude in going from (b) to (a). At $q = \pi$, however, the spectrum gets broadened, as one goes from the Haldane into the Néel phase by changing the anisotropy.

Moving to spectra at $q = \pi$, one can clearly see the sharp magnon peak which dominates the spectrum at all anisotropies and magnetic fields. At zero magnetic field, the peak position which is a fingerprint of the spin gap shifts towards lower frequencies as we go from strong easy-axis anisotropy $D = -0.5J$ in Fig. 5(f) to strong easy-plane anisotropy $D = 0.5J$ in Fig. 5(l). We find that, in all cases studied, there is a good agreement between the position of the peak maxima and the thermodynamic spin gaps which we obtained in Sec. II. As can be seen from Figs. 5(f) through 5(l) the monotonic behavior of the spectrum in terms of anisotropy remains intact, even at finite magnetic field, but it is accompanied by a splitting of the dominant peak due to the Zeeman effect, as we already mentioned in the context of Fig. 4. The splitting increases until the lower branch reaches its maximum at zero frequency, at $h = h_c(D)$, where the LLQ is entered. Increasing the magnetic field beyond $h_c(D)$ leads to an accumulation of spectral weight at zero frequency and a depletion and smearing of the upper

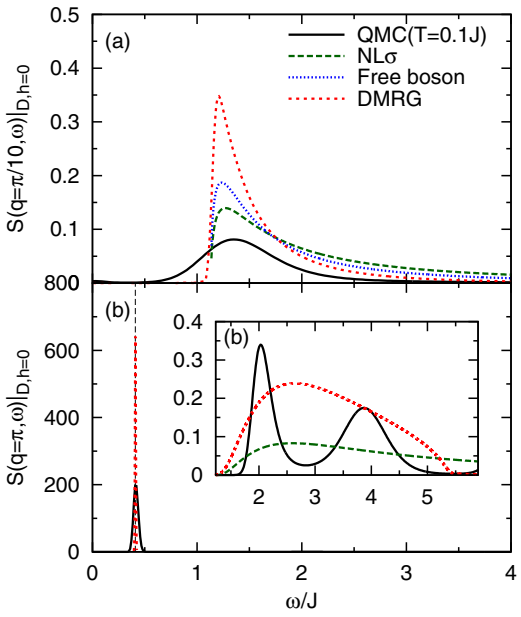

FIG. 6. (Color online) Transverse dynamic structure factor of the isotropic chain, $D = 0$, at zero magnetic field, $h = 0$, for two wave vectors: a) $q = \pi/10$, b) $q = \pi$, and different methods. In inset b), the large-frequency spectra at $q = \pi$ are plotted. For QMC data, the temperature is set to $T = 0.1J$, while for other data which are extracted from Refs. [6,8,13], the temperature is zero.

Zeeman peak. This behavior is clearly visible in Figs. 5(k) and 5(l). In view of the phase diagram Fig. 2, and because the largest field we consider in Fig. 5 is $h_c(0)$, the maximum of the lower branch has to stay above $\omega = 0$ for $D < 0$, which is exactly what we find in Figs. 5(f) and 5(g).

In addition to the dominant single-magnon peak at $q = \pi$, we find a very weak multiparticle continuum at higher frequencies. This is most likely due to three-magnon excitations, as proposed in Refs. [8,13]. In view of the relative intensities, it is remarkable that our MaxEnt calculations are able to resolve this continuum with respect to the single-magnon peak. Moreover, these results hint as to why experimental inelastic structure factor determinations of such continua have failed so far [15].

Finally we contrast our findings with those from other approaches, namely, the NLσ model and a free-boson method [6,8], as well as TDMRG [13]. In Fig. 6 results are shown for two momenta, i.e., $q = \pi/10$ and $q = \pi$. For the former, the spectrum is dominated by only the two-particle continuum and Fig. 6(a) demonstrates good qualitative agreement between all different methods. Regarding the quantitative difference of the QMC results from the other approaches, it is clear that the sharp onset of the continuum is smeared. The reason for this is twofold; primarily it results from the fact that our QMC is a finite-temperature result, at $T = 0.1J$, while all other methods refer to zero temperature. Additionally MaxEnt cannot be avoided for introducing additional smoothing of any QMC spectrum. The spectrum at $q = \pi$ is shown in Fig. 6(b). As discussed previously, this spectrum contains two largely separated intensity scales, one due to the single-magnon mode, the other due to the three-particle continuum. For the former and as for Fig. 6(a) we see convincing agreement between all approaches for the locations of the magnon peak, including some finite-temperature and MaxEnt broadening of the QMC spectrum. Turning to the high-energy continuum at this wave vector, we first note that all methods result in a comparable spectral intensity; however, clear qualitative differences are obvious. While both the NLσ model and TDMRG display only a single "hump," the QMC calculation results in two. Moreover, while the TDMRG and QMC spectra remain confined to $1.5 \lesssim \omega/J \lesssim 5.5$, the spectrum from the NLσ model continues up to much higher energies. The origin of these differences remains unclear at present.

IV. CONCLUSIONS

We have used QMC calculations to study the antiferromagnetic spin-1 chain subject to the simultaneous presence of single-ion anisotropy and external magnetic fields. The focus has been on two issues, namely, the quantum phase diagram and the transverse dynamic structure factor. We have uncovered a rich set of quantum phases within the parameter range investigated, comprising Néel, Haldane, Luttinger-liquid, and large-anisotropy regimes. The gaps and order parameters we have studied show continuous behavior at the Néel to Haldane, as well as the Haldane and large-anisotropy to Luttinger-liquid transitions. The order of the Néel to Luttinger-liquid transition remains an open issue.

Based on the phase diagram, we have determined the transverse spin dynamics covering the complete Brillouin zone, and varied the system parameters to access the excitations within the Néel, Haldane, and Luttinger-liquid states. First, we studied the spectral weight, splitting, and dispersion of the single-magnon mode, known from the standard antiferromagnetic spin-1 chain, but versus anisotropy and external fields. Second, we have provided clear evidence for multiparticle continua with partially very small spectral weight and investigated their evolution with momentum and system parameters.

Finally we have shown that our finite-temperature spectra are consistent with existing zero-temperature results from other analytic as well as numerical approaches. We hope that our findings may inspire additional experimental studies using inelastic neutron scattering on spin-1 chain materials.

ACKNOWLEDGMENTS

Part of this work has been supported by the Deutsche Forschungsgemeinschaft through SFB 1143, FOR912 Grant No. BR 1084/6-2, the European Commission through MC-ITN LOTHERM Grant No. PITN-GA-2009-238475, and the NTH School for Contacts in Nanosystems. W.B. thanks the Platform for Superconductivity and Magnetism, Dresden, where part of this work was performed, for its kind hospitality.

APPENDIX: METHOD

All physical quantities in this paper are obtained using the stochastic series expansion method, pioneered by Sandvik *et al.* [56–58]. This method is based on importance sampling of the high-temperature series expansion of the partition

function

$$Z = \sum_{\alpha} \sum_{n} \sum_{S_n} \frac{(-\beta)^n}{n!} \langle \alpha | \prod_{k=1}^{n} H_{a_k,b_k} | \alpha \rangle , \qquad \text{(A1)}$$

where β is the inverse temperature $1/T$, and $H_{1,b} = 1/2 - S^z_{b1} S^z_{b2}$ and $H_{2,b} = (S^+_{b1} S^-_{b2} + S^-_{b1} S^+_{b2})/2$ are spin-diagonal and off-diagonal bond operators. $|\alpha\rangle = |S^z_1, \ldots, S^z_N\rangle$ refers to the S^z basis and $S_n = [a_1,b_1][a_2,b_2]\cdots[a_n,b_n]$ is an index for the operator string $\prod_{k=1}^{n} H_{a_k,b_k}$. This string is Metropolis sampled, using two types of update, diagonal updates which change the number of diagonal operators H_{1,b_k} in the operator string and directed loop updates which change the type of operators $H_{1,b_k} \leftrightarrow H_{2,b_k}$. For nonfrustrated spin systems the latter update comprises an even number of off-diagonal operators H_{2,b_k}, ensuring positivity of the transition probabilities.

The dynamic structure factor is obtained from the QMC calculation in real space i,j and at imaginary time τ. Following Ref. [56] we consider the corresponding correlators

$$S^{\pm\mp}_{i,j}(\tau) = \left\langle \sum_{p,m=0}^{n} \frac{\tau^m (\beta-\tau)^{n-m} n!}{\beta^n (n+1)(n-m)! m!} \times S^{\pm}_i(p) S^{\mp}_j(p+m) \right\rangle_W , \qquad \text{(A2)}$$

where $\langle \cdots \rangle_W$ refers to the Metropolis weight of an operator string of length n generated by the stochastic series expansion of the partition function [57,58], p,m are positions in this string and $S_i(p)$ refers to the intermediate state $|\alpha(p)\rangle = \prod_{k=1}^{p} H_{a_k,b_k} |\alpha\rangle$. The $S^{xx(yy)}_{i,j}(\tau)$ correlators can be derived from (A2).

The dynamic structure factor at imaginary times and in momentum space is obtained from the Fourier transformation

$$S^{\alpha\beta}(q,\tau) = \sum_{r} e^{iqr} S^{\alpha\beta}_{r,0}(\tau)/L \qquad \text{(A3)}$$

with L being the system size. The sought-for form of the dynamical structure factor in frequency and momentum space finally results from analytic continuation to real frequencies based on the inversion of

$$S^{\alpha\beta}(q,\tau) = \frac{1}{\pi} \int_0^{\infty} d\omega \; S^{\alpha\beta}(q,\omega) K(\omega,\tau), \qquad \text{(A4)}$$

with a kernel $K(\omega,\tau) = e^{-\tau\omega} + e^{-(\beta-\tau)\omega}$.

The preceding inversion is an ill-posed problem, for which maximum entropy methods (MaxEnt) have proven to be well suited. We have applied Bryan's algorithm for our MaxEnt [59,60]. In a nutshell this method minimizes the functional $Q = \chi^2/2 - \alpha\sigma$, with χ being the covariance of the QMC data with respect to the MaxEnt trial spectrum $S(q,\omega)$. Overfitting is prevented by an entropy term $\sigma = \sum_{\omega} S(q,\omega) \ln[S(q,\omega)/m(\omega)]$. We have used a flat default model $m(\omega)$ which is iteratively adjusted to match the zeroth moment of the trial spectrum. The optimal spectrum follows from the weighted average of $S(q,\omega)$ with the probability distribution $P[\alpha|S(q,\tau)]$ adopted from Ref. [59]. Using static structure factors evaluated by independent QMC runs, we have checked that all spectra obtained from our MaxEnt perfectly fulfill sum rules.

[1] F. D. M. Haldane, Phys. Rev. Lett. **50**, 1153 (1983).
[2] H.-J. Mikeska and A. K. Kolezhuk, Lect. Notes Phys. **645**, 1 (2004).
[3] M. P. Nightingale and H. W. J. Blöte, Phys. Rev. B **33**, 659 (1986).
[4] S. R. White and D. A. Huse, Phys. Rev. B **48**, 3844 (1993).
[5] G. Gómez-Santos, Phys. Rev. Lett. **63**, 790 (1989).
[6] I. Affleck and R. A. Weston, Phys. Rev. B **45**, 4667 (1992).
[7] S. Yamamoto and S. Miyashita, Phys. Rev. B **48**, 9528 (1993).
[8] M. D. P. Horton and I. Affleck, Phys. Rev. B **60**, 11891 (1999).
[9] M. Takahashi, Phys. Rev. Lett. **62**, 2313 (1989).
[10] J. Deisz, M. Jarrell, and D. L. Cox, Phys. Rev. B **42**, 4869 (1990).
[11] S. V. Meshkov, Phys. Rev. B **48**, 6167 (1993).
[12] S. Yamamoto and S. Miyashita, Phys. Lett. A **235**, 545 (1997).
[13] S. R. White and I. Affleck, Phys. Rev. B **77**, 134437 (2008).
[14] S. Ma, C. Broholm, D. H. Reich, B. J. Sternlieb, and R. W. Erwin, Phys. Rev. Lett. **69**, 3571 (1992).
[15] I. A. Zaliznyak, S.-H. Lee, and S. V. Petrov, Phys. Rev. Lett. **87**, 017202 (2001).
[16] M. Kenzelmann, R. A. Cowley, W. J. L. Buyers, R. Coldea, J. S. Gardner, M. Enderle, D. F. McMorrow, and S. M. Bennington, Phys. Rev. Lett. **87**, 017201 (2001).
[17] J. P. Renard, M. Verdaguer, L. P. Regnault, W. A. C. Erkelens, J. Rossat-Mignod, and W. G. Stirling, Europhys. Lett. **3**, 945 (1987).
[18] L. P. Regnault, I. Zaliznyak, J. P. Renard, and C. Vettier, Phys. Rev. B **50**, 9174 (1994).
[19] A. Paduan-Filho, X. Gratens, and N. F. Oliveira, Phys. Rev. B **69**, 020405 (2004).
[20] V. S. Zapf, D. Zocco, B. R. Hansen, M. Jaime, N. Harrison, C. D. Batista, M. Kenzelmann, C. Niedermayer, A. Lacerda, and A. Paduan-Filho, Phys. Rev. Lett. **96**, 077204 (2006).
[21] M. Orendáč, A. Orendáčová, J. Černák, A. Feher, P. J. C. Signore, M. W. Meisel, S. Merah, and M. Verdaguer, Phys. Rev. B **52**, 3435 (1995).
[22] Z. Honda, H. Asakawa, and K. Katsumata, Phys. Rev. Lett. **81**, 2566 (1998).
[23] A. Zheludev, Y. Chen, C. L. Broholm, Z. Honda, and K. Katsumata, Phys. Rev. B **63**, 104410 (2001).
[24] Z. Honda, K. Katsumata, H. Aruga Katori, K. Yamada, T. Ohishi, T. Manabe, and M. Yamashita, J. Phys.: Condens. Matter **9**, L83 (1997).
[25] A. Zheludev, Z. Honda, K. Katsumata, R. Feyerherm, and K. Prokes, Europhys. Lett. **55**, 868 (2001).
[26] M. Steiner, K. Kakurai, J. K. Kjems, D. Petitgrand, and R. Pynn, J. Appl. Phys. **61**, 3953 (1987).

[27] M. Kenzelmann, R. A. Cowley, W. J. L. Buyers, Z. Tun, R. Coldea, and M. Enderle, Phys. Rev. B **66**, 024407 (2002).
[28] A. Zheludev, S. M. Shapiro, Z. Honda, K. Katsumata, B. Grenier, E. Ressouche, L.-P. Regnault, Y. Chen, P. Vorderwisch, H.-J. Mikeska, and A. K. Kolezhuk, Phys. Rev. B **69**, 054414 (2004).
[29] M. Sieling, U. Löw, B. Wolf, S. Schmidt, S. Zvyagin, and B. Lüthi, Phys. Rev. B **61**, 88 (2000).
[30] S. A. Zvyagin, J. Wosnitza, A. K. Kolezhuk, V. S. Zapf, M. Jaime, A. Paduan-Filho, V. N. Glazkov, S. S. Sosin, and A. I. Smirnov, Phys. Rev. B **77**, 092413 (2008).
[31] M. Chiba, Y. Ajiro, H. Kikuchi, T. Kubo, and T. Morimoto, Phys. Rev. B **44**, 2838 (1991).
[32] M. Takigawa, T. Asano, Y. Ajiro, M. Mekata, and Y. J. Uemura, Phys. Rev. Lett. **76**, 2173 (1996).
[33] N. Haga and S.-i. Suga, J. Phys. Soc. Jpn. **69**, 2431 (2000).
[34] A. V. Sologubenko, T. Lorenz, J. A. Mydosh, A. Rosch, K. C. Shortsleeves, and M. M. Turnbull, Phys. Rev. Lett. **100**, 137202 (2008).
[35] M. den Nijs and K. Rommelse, Phys. Rev. B **40**, 4709 (1989).
[36] H. J. Schulz, Phys. Rev. B **34**, 6372 (1986).
[37] T. Kennedy and H. Tasaki, Commun. Math. Phys. **147**, 431 (1992).
[38] W. Chen, K. Hida, and B. C. Sanctuary, Phys. Rev. B **67**, 104401 (2003).
[39] C. Degli Esposti Boschi, E. Ercolessi, F. Ortolani, and M. Roncaglia, Eur. Phys. J. B **35**, 465 (2003).
[40] Y.-C. Tzeng and M.-F. Yang, Phys. Rev. A **77**, 012311 (2008).
[41] S. Hu, B. Normand, X. Wang, and L. Yu, Phys. Rev. B **84**, 220402 (2011).
[42] S. C. Furuya, T. Suzuki, S. Takayoshi, Y. Maeda, and M. Oshikawa, Phys. Rev. B **84**, 180410 (2011).
[43] A. F. Albuquerque, C. J. Hamer, and J. Oitmaa, Phys. Rev. B **79**, 054412 (2009).
[44] I. Affleck, Phys. Rev. B **43**, 3215 (1991).
[45] O. Golinelli, T. Jolicoeur, and R. Lacaze, Phys. Rev. B **45**, 9798 (1992).
[46] R. M. Konik and P. Fendley, Phys. Rev. B **66**, 144416 (2002).
[47] F. Pollmann, A. M. Turner, E. Berg, and M. Oshikawa, Phys. Rev. B **81**, 064439 (2010).
[48] Z.-C. Gu and X.-G. Wen, Phys. Rev. B **80**, 155131 (2009).
[49] P. Sengupta and C. D. Batista, Phys. Rev. Lett. **99**, 217205 (2007).
[50] V. Zapf, M. Jaime, and C. D. Batista, Rev. Mod. Phys. **86**, 563 (2014).
[51] C. Psaroudaki, S. A. Zvyagin, J. Krzystek, A. Paduan-Filho, X. Zotos, and N. Papanicolaou, Phys. Rev. B **85**, 014412 (2012).
[52] F. Anfuso and A. Rosch, Phys. Rev. B **76**, 085124 (2007).
[53] M. N. Barber, *Phase Transitions and Critical Phenomena* (Academic Press, London, 1983).
[54] D. Charrier, S. Capponi, M. Oshikawa, and P. Pujol, Phys. Rev. B **82**, 075108 (2010).
[55] Y. H. Su, S. Y. Cho, B. Li, H.-L. Wang, and H.-Q. Zhou, J. Phys. Soc. Jpn. **81**, 074003 (2012).
[56] A. W. Sandvik, J. Phys. A: Math. Gen. **25**, 3667 (1992).
[57] A. W. Sandvik, Phys. Rev. B **59**, R14157 (1999).
[58] O. F. Syljuasen and A. W. Sandvik, Phys. Rev. E **66**, 046701 (2002).
[59] R. K. B. J. Skilling, Mon. Not. R. Astron. Soc. **211**, 111 (1984).
[60] M. Jarrell and J. Gubernatis, Phys. Rep. **269**, 133 (1996).